Investigation of a New Cyclotriphosphazene-Terminated Perfluoropolyether Lubricant. Properties and Interactions with a Carbon Surface

R. J. Waltman,*,† D. J. Pocker,† and H. Deng†

IBM Storage and Technology Division, 5600 Cottle Road, San Jose, California 95193

N. Kobayashi, Y. Fujii, T. Akada, and K. Hirasawa

Matsumura Oil Research Corporation, 5-3, Minatojima Minami-machi 5-Chome, Chuo-ku, Kobe, Hyogo 650-0047, Japan

G. W. Tyndall

IBM Almaden Research Center, 650 Harry Road, San Jose, California 95120

Received October 24, 2002. Revised Manuscript Received March 24, 2003

A novel perfluoropolyether (PFPE) structure terminated on one chain end by a hydroxyl end group and on the other end by a cyclotriphosphazene derivative was studied. The interactions that developed at the interface between molecularly thin films of this material (A20H) and amorphous nitrogenated carbon surfaces were investigated using contact angle goniometry, Fourier transform infrared spectroscopy, X-ray photoelectron spectroscopy, and imaging ellipsometry. The results demonstrate that both the cyclotriphosphazene and the hydroxyl end group of monolayer A20H films are capable of attractive interactions with the carbon surface. These interactions induce a layering in the adsorbed film that is manifested in an oscillatory dependence of the surface free energy on applied A20H film thickness. The thickness of the first A20H monolayer is determined from the first minimum in the surface energy to be 13.0 ± 1.0 Å for the 2400 molecular weight material and 15.0 ± 1.0 Å for the 3100 molecular weight material studied. The second A20H monolayer is not completely wetting on the first monolayer. This results in an autophobic dewetting when A20H films in excess of the monolayer thickness are applied to the carbon surface. The mobilities of A20H monolayer films were also qualitatively compared to that of the hydroxyl-terminated PFPE, Fomblin Zdol. While interaction of the cyclotriphosphazene end group with the carbon surface increases the load-bearing capability of the PFPE film when compared to Zdol, it also has the effect of decreasing the mobility of the adsorbed film.

Introduction

The successful operation of a hard-disk drive product is critically dependent upon the formation of a tribologically robust interface between the read−write head and the magnetic recording disk. In brief, a magnetic recording device relies on flying a slider containing the read−write elements (i.e., "head") over a rotating disk at separation distances (fly heights) on the order of tens of nanometers or less. To minimize the wear resulting from any high-speed intermittent contacts between these two surfaces, the magnetic recording disk and the read−write head are typically overcoated with a hard amorphous carbon film and the surface of the disk is lubricated with a molecularly thin film of a perfluoropolyether (PFPE) oil of relatively low molecular weight ($M_n \leq \sim 5000$). The most commonly employed PFPE used for magnetic recording applications is Fomblin Zdol,

$$HO-CH_2CF_2O-[CF_2O]_x-[CF_2CF_2O]_y-CF_2CH_2-OH$$

While this material has been successfully used in the computer disk industry for over a decade, it is unclear whether it will be capable of meeting the increasingly stringent demands that will be placed on the lubricant in future storage devices.

The durability of the head−disk interface in magnetic storage devices is contingent upon a number of factors. Arguably foremost among these is the relative mobility of the PFPE lubricant on the carbon overcoat. Upon contact of the head with the disk surface, the lubricant film can become displaced or depleted if the contact force exceeds the load-bearing capability of the lubricant. Highly mobile lubricant systems are generally characterized by lower load-bearing capabilities, which is undesirable since lubricant thinning can degrade the durability of the head−disk interface.[1] Conversely, a lubricant film characterized by a high degree of mobility

* To whom correspondence should be addressed.
† Present address: Hitachi Global Storage Technology, 5600 Cottle Road, San Jose, CA 95193.

(1) Chen, C.-Y.; Fong, W.; Bogy, D. B.; Bhatia, C. S. *Tribol. Lett.* **1999**, *7*, 1.

10.1021/cm021048+ CCC: $25.00
Published on Web 05/07/2003

will facilitate the replenishment of lubricant to the locally depleted areas of the disk surface, thereby enhancing the durability exhibited by the interface.[2−4]

In addition to the forces generated upon hard contact between the read−write head and the disk surface, there are a number of other forces acting on the lubricant in hard-disk drives. For example, a positive pressure exists under the flying slider, that is, the air-bearing pressure. The magnitude of the air-bearing pressure is dependent on the slider design and the separation distance (fly height) between the active elements of the read−write head and the magnetic recording disk. At the fly heights utilized in current drives, the air-bearing pressure can approach values exceeding the internal (disjoining) pressure of the confined lubricant film. Under these conditions, hydrostatics will drive a displacement of lubricant from under the flying head, which in turn can adversely effect the lifetime of the head−disk interface.[3] Since the magnitude of the peak pressure under a given slider will scale approximately inversely with the fly height, this phenomenon will become increasingly important in future drives that will require lower fly heights to meet the magnetic recording density requirements. Lubricant depletion and/or redistribution on a disk surface can also result from both the centrifugal force and the wind shear acting on the adsorbed film during drive operation.[3,5] These latter phenomena have been exacerbated in recent years by the increased disk rotation speed (15000 rpm) characteristic of some current hard-disk drive products.

The mobility and load-bearing capability of a molecularly thin PFPE lubricant film are governed by the interactions that develop at the PFPE/carbon interface. It has been shown that the interactions of end-functionalized PFPE lubricants with the carbon surface of magnetic recording disks are characterized by relatively weak dispersion forces between the PFPE backbone and the surface and by the formation of strongly attractive interactions between the end groups and specific chemical functionalities on the carbon surface.[6] The PFPE backbone−surface interactions result in the formation of a disjoining pressure, Π, defined by the gradient in the Gibbs free energy, F, with film thickness, h,[7]

$$\Pi = -\left(\frac{\mathrm{d}F}{\mathrm{d}h}\right)_{\mathrm{T}} \qquad (1)$$

This (negative) pressure that resists film thinning when an external force is applied to the lubricant is strongly dependent on the PFPE film thickness, scaling as h^{-3}. Interaction of the PFPE end groups can also enhance the load-bearing capability of the lubricant by increasing the adhesion of the monolayer film to the carbon surface.[6] In the case of Zdol on amorphous nitrogenated carbon, CNx, for example, the adhesion provided via hydrogen bonding of the hydroxyl end groups to the surface is sufficient to render these polymer chains immobile. While this would be beneficial in limiting the amount of lubricant displacement from under a flying head, the resulting reduction in reflow rate will have a deleterious effect on the interface durability probed in, for example, contact start−stop testing.[2−4]

Attachment of alternative end groups to the PFPE backbone offers the possibility of altering both the nature and the strength of the adhesive interactions with the surface, thereby impacting the tribological performance of the head−disk interface. Recently, mixtures of cyclotriphosphazenes, for example, X-1P (Dow Chemical), and PFPEs have been reported to enhance the interface durability.[8−11] However, a number of concerns arise in using a two-component lubricant system. Possibly foremost among these is the immiscibility of many cyclotriphosphazenes in perfluoropolyethers. This inherent incompatibility can lead to difficulties in ensuring consistent uptake of both components onto the disk surface in a high volume manufacturing application. Furthermore, the limited solubility of the cyclotriphosphazene in the PFPEs could potentially result in a phase separation of the two components on the disk surface during drive operation.[12,13] One means to alleviate these concerns is to incorporate the desired cyclotriphosphazene functionality directly into the PFPE structure. A PFPE material has recently been developed which is terminating on one end with *m*-trifluoromethylphenoxycyclotriphosphazene and on the other end by a hydroxyl moiety. In the current work, we establish the nature of the adhesive interactions that develop between molecularly thin films of this hybrid PFPE and an amorphous nitrogenated carbon surface and quantify the impact of these interactions on the structure, stability, and mobility of the adsorbed film.

Experimental Section

The cyclotriphosphazene-terminated perfluoropolyether lubricant used in this work was synthesized and purified by the Matsumura Oil Research Corporation, Japan. The lubricant is designated "A20H", which is an end-functionalized PFPE based on the Fomblin Z backbone (random copolymer of perfluorethylene oxide and perfluoromethylene oxide repeat units). Two distinct products are formed in the synthesis of A20H. The dominant species (88 ± 2%) is the PFPE backbone terminated on one end by a cyclotriphosphazene ring and on the other end by a hydroxyl moiety. The minor component in A20H is a structure in which both PFPE chain ends are

(2) Chen, C.-Y.; Bogy, D. B.; Bhatia, C. S. *Tribol. Lett.* **2001**, *10*, 195.
(3) Waltman, R. J.; Tyndall, G. W. *J. Magn. Soc. Jpn.* **2002**, *26*, 97.
(4) Karis, T. E.; Tyndall, G. W.; Waltman, R. J. *Tribol. Trans.* **2001**, *44*, 249.
(5) Mate, C. M.; Wilson, R. S. *ACS Symp. Ser.* **2001**, *787*, 83.
(6) Tyndall, G. W.; Waltman, R. J.; Pocker, D. J. *Langmuir* **1998**, *14*, 7527. Waltman, R. J.; Tyndall, G. W.; Pacansky, J. *Langmuir* **1999**, *15*, 6470.
(7) Derjaguin, B. V.; Churaev, N. V. *J. Colloid Interface Sci.* **1974**, *49*, 249. Derjaguin, B. V. *Langmuir* **1987**, *3*, 601, and references therein.
(8) Chen, C.-Y.; Bogy, D. B.; Cheng, T.; Bhatia, C. S. *IEEE Trans. Magn.* **2000**, *36*, 2708.
(9) Yang, M.; Talke, F. E.; Perettie, D. J.; Morgan, T. A.; Kar, K. K.; Dekoven, B.; Potter, G. E. *Tribol. Trans.* **1995**, *38*, 636.
(10) Perettie, D. J.; Johnson, W. D.; Morgan, T. A.; Kar, K. K.; Potter, G. E.; DeKoven, B. M.; Chao, J.; Lee, Y. C.; Gao, C.; Russak, M. In *Advances in Information Storage and Processing Systems*; Adams, G. G., Bhushan, B., Miu, D., Wickert, J., Eds.; ASME: New York, 1995.
(11) Yang, M.; Talke, F. E.; Perettie, D. J.; Morgan, T. A.; Kar, K. K. *IEEE Trans. Magn.* **1994**, *30*, 4143.
(12) Hara, H.; Nishiguchi, I.; Sugi, S.; Tsuboi, S. *Tribol. Lett.* **2001**, *10*, 143. Kang, H.-J.; Perettie, D. J.; Talke, F. E. *IEEE Trans. Magn.* **1999**, *35*, 2385.
(13) Zhao, Q.; Kang, H.-J.; Fu, L.; Talke, F. E.; Perettie, D. J.; Morgan, T. A. STLE Preprint No. 98-TC-4C-1, ASME: New York, 1998.

Table 1. Characterization of A20H Lubricant Lots Used in the Current Studies

	A20H-1	A20H-2
composition	86% Phos−PFPE−OH 14% Phos−PFPE−Phos	90% Phos−PFPE−OH 10% Phos−PFPE−Phos
number-average mol. wt. (M_n)	2400 (Pho−-PFPE−OH) 3330 (Phos−PFPE−Phos)	3100 (Phos−PFPE−OH) 4050 (Phos−PFPE−Phos)
polydispersity (M_w/M_n)	1.41	1.04 (Phos−PFPE−OH) 1.02 (Phos−PFPE−Phos)
C1/C2	0.8	0.87

terminated with cyclotriphosphazene groups. The structure of both the major (Phos−PFPE−OH) and minor (Phos−PFPE−Phos) components are schematically shown below.

A20H

Major Component:

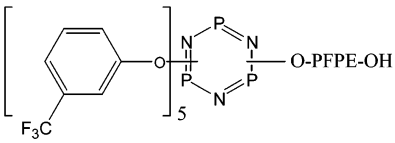

Minor Component:

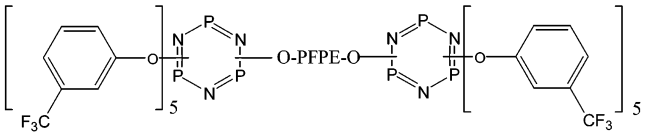

The results from two samples, designated A20H-1 and A20H-2, respectively, are reported below. In the first sample, A20H-1, the number-average molecular weight, M_n, of the majority component (Phos−PFPE−OH) is 2400 and that of the minority component is nominally 3350. This sample is polydisperse with a polydispersity index (ratio of the weight-average to number-average molecular weights, M_w/M_n) of 1.41. The ratio of perfluoromethylene oxide to perfluoroethylene oxide repeat units in the PFPE backbone is found by NMR to be 0.8. This sample was used as received. The second sample, designated A20H-2, was fractionated via CO_2 supercritical fluid extraction. The majority component, Phos−PFPE−OH, is characterized by a number-average molecular weight of 3100 and a polydispersity of $M_w/M_n = 1.04$. The average molecular weight of the minority component in A20H-2 is 4000. These data are summarized in Table 1.

The lubricants were applied to magnetic recording disks from solutions of the A20H samples in hydrofluoroether (HFE-7100, 3M) using standard dip-coating techniques. The disks utilized in this work were comprised of a super-smooth glass substrate (RMS roughness of ≤10 Å), onto which was sputter-deposited an underlayer of Cr, a Cobalt-based magnetic layer, and nominally 50 Å of amorphous nitrogenated carbon (CN*x*). The nitrogen concentration in the carbon overcoat was found to be 12 at. % as determined via X-ray photoelectron spectroscopy (XPS). Additionally, XPS experiments conducted near the grazing exit indicate that the CN*x* surface is highly oxidized (10 at. % oxygen) and depleted in nitrogen compared to the bulk.

The lubricant films were characterized using XPS and FTIR. The XPS measurements were made on a Phi Quantum 2000 ESCA System employing monochromatic Al Kα irradiation. Measurements were conducted using three takeoff angles: standard (45 ± 15°), near perpendicular (75−90°), and grazing (0−17°). The standard takeoff angle was used to determine the thickness of the Phos−PFPE−OH film,[14] and the near perpendicular and grazing takeoff angle measurements were used to obtain information on the structure of the adsorbed Phos−PFPE−OH film. FTIR was also used to quantify the

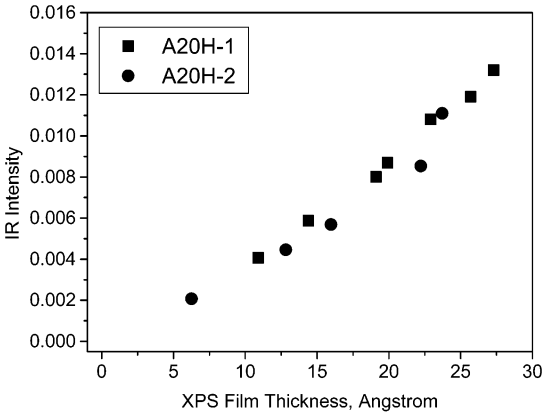

Figure 1. Relationship between the IR intensity of the 1262 cm^{-1} band in A20H versus the film thickness as determined by XPS measurements.

applied film thickness. As shown in Figure 1, a linear relationship between the intensity of the absorbance band centered at 1262 cm^{-1} and the film thickness determined from the XPS measurements is observed.

Contact angle measurements were used to obtain the surface energies of unlubricated and A20H-lubricated CN*x* disks. The total free energy of a surface can be written as a sum of separable components

$$\gamma_s = \gamma_s^d + \gamma_s^p + ... \quad (2)$$

where γ_s^d and γ_s^p are the dispersive and polar components of the free energy, respectively.[15] The contact angle, θ, made between a liquid and a solid surface is related to the free energy of the surface, γ_s, via Young's equation

$$\gamma_1 \cos\theta = \gamma_s - \gamma_{sl} \quad (3)$$

where γ_1 is the surface energy (tension) of the reference liquid and γ_{sl} is the solid−liquid interfacial energy. The dispersive component of the surface energy is determined from contact angle measurements conducted with reference liquids capable of interacting with the surface via dispersive forces only. In this case, the solid−liquid interfacial energy, γ_{sl}, is given by[16,17]

$$\gamma_{sl}^d = \gamma_s^d + \gamma_1^d - 2\sqrt{\gamma_s^d \gamma_1^d} \quad (4)$$

The dispersive component of the surface energy is then obtained by the substitution of eq 4 into eq 3:

$$\gamma_s^d = \frac{\gamma_1^d(1+\cos\theta)^2}{4} \quad (5)$$

When the reference liquid is capable of interacting with the surface via both dispersive and polar forces, the interfacial energy can be approximated by[18,19]

$$\gamma_{sl} = \gamma_s + \gamma_1 - 2\sqrt{\gamma_s^d \gamma_1^d} - 2\sqrt{\gamma_s^p \gamma_1^p} \quad (6)$$

which upon substitution into Youngs equation readily yields an expression for the polar component of the surface energy.

The dispersive component of the free energy for the bare CN*x* surface studied in the current work was determined from

(14) Toney, M. F.; Mate, C. M.; Pocker, D. J. *IEEE Trans. Magn.* **1998**, *34*, 1774.
(15) Fowkes, F. M. *Ind. Eng. Chem.* **1964**, *56*, 40.
(16) Wu, S. *Polymer Interface and Adhesion*; Marcel Dekker: New York, 1982.
(17) Adamson, A. W. *Physical Chemistry of Surfaces*, 5th ed.; John Wiley and Sons: New York, 1990.
(18) Owens, D. K.; Wendt, R. D. *J. Appl. Polym. Sci.* **1969**, *13*, 741.
(19) Kaelble, D. H. *J. Adhes.* **1970**, *2*, 66.

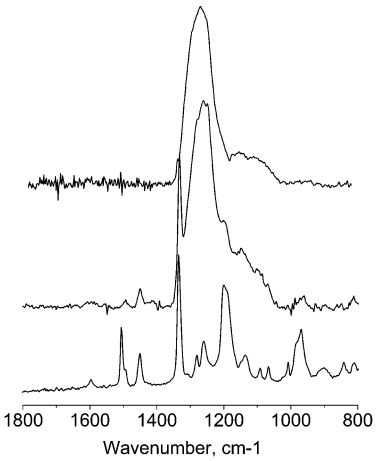

Figure 2. IR spectra for (top) 8 Å Zdol 4000, (middle) 10 Å A20H-1, and (bottom) 6 Å X-1P.

eq 4 using methylene iodide ($\gamma_1^d \approx \gamma_1 = 51$ mJ/m^2)[20] as the reference liquid. The dispersive component of the free energy for the A20H-lubricated surfaces was determined as a function of A20H film thickness using a series of saturated *n*-alkanes as the reference liquids.[21] The polar component of the surface energy for both the bare CN*x* surface and the A20H-lubricated CN*x* surfaces were then determined using the experimentally determined dispersive surface energies and the contact angles made with the surface using water ($\gamma_1^d = 21.8$ mJ/m^2 and $\gamma_1^p = 51.0$ mJ/m^2) as the reference liquid.[22] The total surface energy is then simply obtained by summing these two components.

The stability and mobility of molecularly thin A20H lubricant films on the CN*x* surface were probed using an optical surface analyzer (Candela Instruments, Fremont, CA). A detailed description of this instrument is available elsewhere.[23] In brief, circularly polarized light from a HeNe laser is reflected off the surface of the disk at nominally Brewster's angle. The specularly reflected light is then collected using a series of detectors. In the current work, the ellipsometric portion of this instrument, namely, the Q polarized wave (phase contrast signal between the p- and s-polarized light), was used to obtain the images shown below.[23]

The bonding and evaporation kinetics of monolayer A20H films on CN*x* overcoated magnetic recording disks were studied as a function of temperature. Following A20H application, the initial film thickness is measured via specular reflectance FTIR. The lubricated disks are then annealed for a specified period of time and the lubricant film thickness remeasured. Any decrease in the total lubricant thickness following this anneal step is attributed to film evaporation from the surface. In the following, we define the evaporated fraction as the decrease in the A20H film thickness normalized to the initial thickness. After determination of the evaporated fraction, the disks are washed in hydrofluoroether to remove any soluble lubricant. In the following, we refer to that component of the A20H film removed by the solvent wash as "mobile" lubricant and that retained by the disk as "bonded" lubricant. The bonded and mobile fractions reported are obtained by ratioing each of these components to the initial total film thickness.

Results

1. FTIR and XPS Analysis of A20H. The specular reflectance infrared spectrum of a 10-Å film of A20H-1 on CN*x* is shown in Figure 2. The infrared spectra of an 8 Å Zdol 4000 film on CN*x* and a 6-Å film of the phosphazine X-1P (Dow Chemical) are also shown in Figure 2 for comparison. The major absorption band in A20H-1 is centered at 1262 cm^{-1}. This broad absorbance is also observed in the IR spectrum of Zdol and is attributed to the combination of C−F and C−O stretching vibrations of the perfluorinated ether backbone. A20H-1 also displays a rather sharp absorbance band near 1330 cm^{-1}. This absorbance, which is absent in Zdol, is also observed in the spectrum of X-1P and is assigned to the C−F stretch of the terminal trifluoromethylphenoxycyclotriphosphazene end group. Additional absorption bands in the A20H-1 film are observed on both the low- and high-frequency sides of the main absorbance at 1262 cm^{-1}. These can be assigned to the cyclotriphosphazene phenyl C═C stretch (1605, 1500, 1450 cm^{-1}), phenyl C−O stretch (1200 cm^{-1}), and the P−O stretch (970 cm^{-1}). We note that the infrared spectrum of A20H-2 is nominally identical to that of A20H-1 shown in Figure 2.

Table 2. XPS Peak Assignments for the A20H/CN*x* Interface

atom	binding energy (eV)	structural assignment
carbon, C(1s)		
(a) *C*−(C,H,N,O)	284.7	CN*x* overcoat, phenoxy ligands (A20H)
(b) *C*−(F_2O, F_3)	292.7	perfluoroethylene oxide in PFPE backbone and trifluoromethyl groups in end group
(c) *C*−(F_2O_2)	294.3	perfluoromethylene oxide in PFPE
oxygen, O(1s)		
(a) *O*−CF_x	532.8	ether oxygens in PFPE backbone
(b) *O*−(non-CF*x*)	535.3	overcoat oxide layer + A20H end group
phosphorus, P(2p)	134.1	cyclotriphosphazene in A20H end group
fluorine, F(1s)	688.7	PFPE backbone and trifluoromethyl in A20H end group
nitrogen, N(1s)	398.3−400.3	CN*x* overcoat, cyclotriphosphazene

XPS measurements were performed on molecularly thin A20H films (23 ± 1 Å) adsorbed onto CN*x* surfaces. As summarized in Table 2, the spectra are comprised of peaks assignable to both the A20H film and the underlying carbon overcoat. The phosphorus P(2p) peak at a binding energy (B.E.) of 134.1 eV and the fluorine F(1s) at a B.E. = 688.7 eV can be unequivocally assigned to the A20H lubricant film as neither of these species are present in the sputtered carbon overcoat. The N(1s), C(1s), and O(1s) signals, however, originate from both the lubricant film and the underlying carbon overcoat. The signal emanating from the lubricant film can in the case of the N(1s) and C(1s) be deconvoluted from those of the surface via examination of the high-resolution spectra. The high-resolution scan of the C(1s) spectral region shown in Figure 3 reveals the presence of two broad peaks. The low B.E. peak at 284.7 eV is strongly asymmetric with a substantial tail extending to higher binding energies. This peak results from photoelectrons emanating from carbon atoms in a variety of bonding environments including carbon bound to carbon, hydrogen, nitrogen, and oxygen. We designate this peak *C*−(C,H,N,O). The higher binding energy peaks (B.E. = 292.7−294.3 eV) derive from carbon atoms

(20) Fowkes, F. M., *J. Adhes. Sci. Technol.* **1987**, *1*, 7.
(21) Fowkes, F. M. In *Chemistry and Physics of Interfaces*; American Chemical Society: Washington, DC, 1965.
(22) Good, R. J.; Chaudhury, M. K.; van Oss, C. J. *Fundamentals of Adhesion*; Plenum Press: New York, 1991.
(23) Cheng, T.; Zhao, B.; Chao, J.; Meeks, S. W.; Velidandea, V. *Tribol. Lett.* **2000**, *9*, 181.

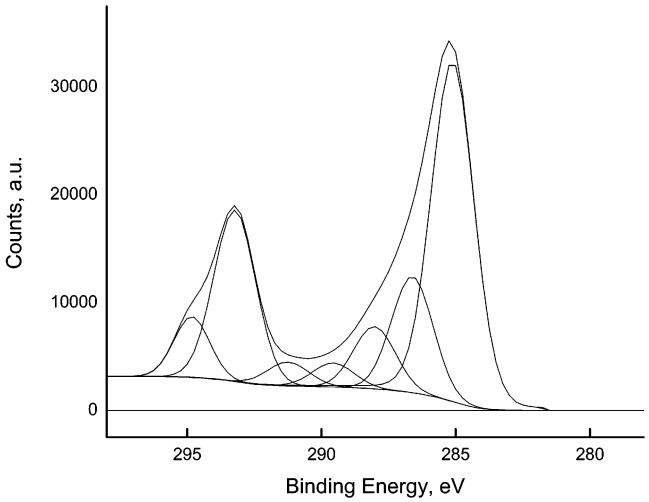

Figure 3. C(1s) XPS spectrum for 23 Å A20H-1 on 50 Å of CN*x* (10 at. % N).

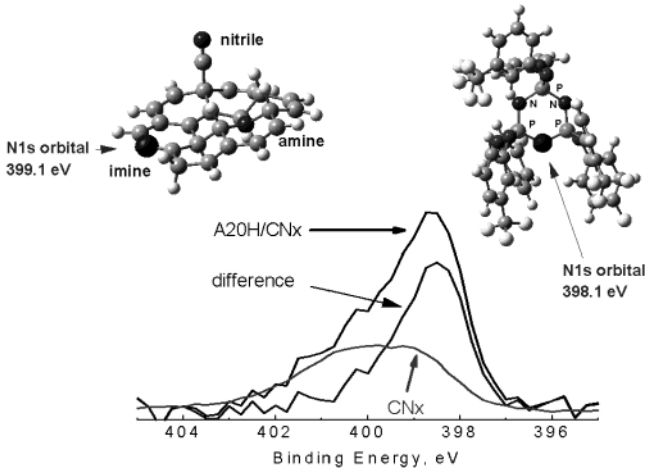

Figure 4. Experimental XPS N(1s) binding energies for 23 Å A20H-1/CN*x* and "bare" CN*x*. The difference spectrum, attributed to A20H-1, has a binding energy of 398.4 eV. The bare CN*x* has a binding energy of ∼399−401 eV. The SCF/3-21G[d] optimized CN*x* (top left) and X-1P (top right) clusters and their computed ionization potentials are also shown above the XPS spectra. The N(1s) one-electron orbital contours corresponding to the ionization is also presented for the imine (CN*x*) and N(═P) nitrogen atoms in the optimized CN*x* and X-1P geometries.

bound to strongly electron-withdrawing F− and CF_x moieties. The lower binding energy peak at 292.7 eV is attributed to the perfluoroethylene oxide repeat units in the PFPE backbone, $-CF_2-\mathit{C}F_2-O$, and the perfluoromethyl groups, $-\mathit{C}F_3$, in the phosphazene end group. The highest energy C(1s) peak at 294.3 eV is assigned to the perfluoromethylene oxide, $-\mathit{C}F_2-O-$, repeat units in the PFPE backbone.

The high-resolution nitrogen (1s) spectra obtained from the A20H film adsorbed on the CN*x* surface and the bare CN*x* surface are shown in Figure 4. Also shown in Figure 4 is the difference spectrum between these two spectra, which can be attributed to the nitrogen in the *m*-trifluoromethylphenoxycyclotriphosphazene end group of A20H. These results clearly demonstrate that the nitrogen in the cyclotriphosphazene end group of A20H is shifted to lower binding energies compared to that of the CN*x* overcoat. This is indicative of nitrogen atoms in substantially different bonding environments.

Table 3. Computed Atomic Charges and Molecular Orbital Energies for the SCF/3-21G[d] Optimized X-1P and CN*x* Clusters Shown in Figure 4

N 1s	orbital energy, a.u.	ionization energy, eV (scaled *x* 0.947)	partial atomic charge (ChelpG)
CN*x* cluster:			
nitrile	−15.489	399.1	−0.67
imine	−15.489	399.1	−0.93
amine	−15.476	398.8	−0.52
X-1P:			
N(═P)	−15.449	398.1	−1.10

The XPS results suggest that the nitrogen atom in the cyclotriphosphazene end group accumulates excess negative charge compared to the nitrogen in the CN*x* overcoat. This was confirmed via ab initio calculations performed on an isolated cyclotriphosphazene (X-1P) and a model CN*x* cluster. The optimized structures of these moieties are shown in Figure 4. The partial atomic charges were computed at the SCF/3-21G[d] level of theory[24] using the ChelpG method.[25] The computed orbital energies and partial atom charges for the respective N(1s) one-electron wave functions in the X-1P and CN*x* clusters are summarized in Table 3. These data indicate a considerably larger charge accumulation on the cyclotriphosphazene nitrogen atoms of X-1P compared to either the amine, imine, or nitrile nitrogen atoms present in the CN*x* model cluster. Also included in Table 3 are the ionization energies obtained assuming Koopmans' theorem. The calculations indicate that the N(1s) B.E. of the cyclotriphosphazene is ∼1 eV smaller than the nitrogen moieties on the model CN*x* cluster. This is in qualitative agreement with the XPS results presented in Figure 4.

Two peaks are also observed in the O(1s) signal at the binding energies of 532.8 and 535.3 eV. The high binding energy peak is attributed to oxygen in the PFPE backbone, designated $\mathit{O}-CF_2$, and the low binding energy peak is assigned to oxygen in the A20H end groups, as well as the oxygen functionalities present on the carbon surface. No attempt was made to deconvolute this latter peak.

Insight into the conformation of the A20H films adsorbed on CN*x* surfaces was obtained via multiple-angle XPS measurements. In these experiments two takeoff angles, grazing (0−17°) and near-perpendicular (75−90°), were employed. In Figure 5 we present the high-resolution C(1s) spectra collected at the grazing exit with that obtained at the near-perpendicular exit. Upon decreasing of the takeoff angle, the relative intensity of those peaks dominated by the carbon overcoat, that is, N(1s), $\mathit{O}-$(non-CF_x) and $\mathit{C}-$(non-CF_x),

(24) Frisch, M. J.; Trucks, G. W.; Schlegel, H. B.; Scuseria, G. E.; Robb, M. A.; Cheeseman, J. R.; Zakrzewski, V. G.; Montgomery, Jr., J. A.; Stratmann, R. E.; Burant, J. C.; Dapprich, S.; Millam, J. M.; Daniels, A. D.; Kudin, K. N.; Strain, M. C.; Farkas, O.; Tomasi, J.; Barone, V.; Cossi, M.; Cammi, R.; Mennucci, B.; Pomelli, C.; Adamo, C.; Clifford, S.; Ochterski, J.; Petersson, G. A.; Ayala, P. Y.; Cui, Q.; Morokuma, K.; Malick, D. K.; Rabuck, A. D.; Raghavachari, K.; Foresman, J. B.; Cioslowski, J.; Ortiz, J. V.; Baboul, A. G.; Stefanov, B. B.; Liu, G.; Liashenko, A.; Piskorz, P.; Komaromi, I.; Gomperts, R.; Martin, R. L.; Fox, D. J.; Keith, T.; Al-Laham, M. A.; Peng, C. Y.; Nanayakkara, A.; Gonzalez, C.; Challacombe, M.; Gill, P. M. W.; Johnson, B.; Chen, W.; Wong, M. W.; Andres, J. L.; Head-Gordon, M.; Replogle, E. S.; Pople, J. A. *Gaussian 98*, Revision A.7; Gaussian Inc.: Pittsburgh, PA, 1998.

(25) Breneman, C. M.; Wiberg, K. B. *J. Comput. Chem.* **1990**, *11*, 361. (b) Chirlian, L. E.; Francl, M. M. *J. Comput. Chem.* **1987**, *8*, 894.

Table 4. Composition of A20H-1 and A20H-2 Films on CN*x* as Determined from XPS[a]

	A20H-1		A20H-2		ratio (grazing/perpendicular)	
species	perpendicular (at. %)	grazing (at. %)	perpendicular (at. %)	grazing (at. %)	A20H-2	A20H-1
N	4.55	1.60	5.71	1.21	0.35	0.21
C−(H,N,O,C)	32.17	14.91	40.55	11.76	0.46	0.29
O−(non-CF*x*)	5.06	3.11	5.74	2.06	0.61	0.36
P	0.76	0.90	0.36	0.42	1.18	1.17
C−(F_3,F_2O_2,F_2O)	13.58	20.07	9.89	19.59	1.48	1.98
F	34.51	46.85	27.16	50.55	1.36	1.86
O−CF_2	8.97	12.55	7.00	14.14	1.40	2.02

[a] A20H-1 measurements conducted at take-off angles of 15 ± 15° (grazing exit) and 75−90° (perpendicular exit). Take-off angles used on A20H-2 film were 0−17° (grazing) and 75−90° (perpendicular).

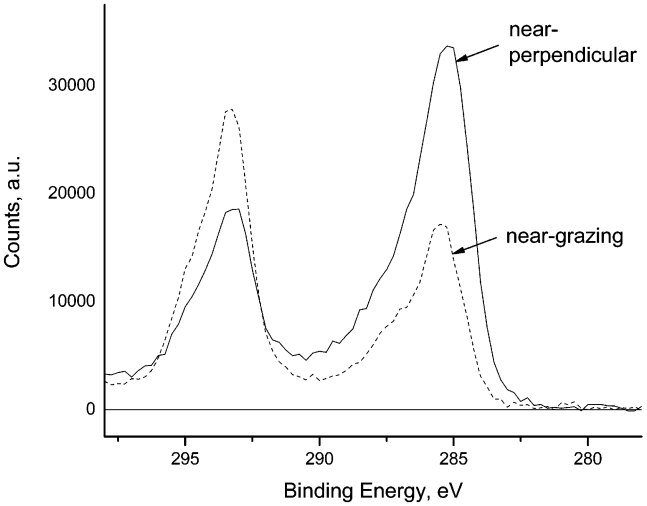

Figure 5. Comparison of the XPS C(1s) near-perpendicular and -grazing take-off angles for the 23 Å A20H-1 film on CN*x*.

decrease while those deriving from the A20H lubricant film, for example, F(1s), *O*−(CF_x), and *C*−(CF_x), increase, as summarized in Table 4. As discussed above, the P(2p) and the fluorine-containing signals, F(1s), *O*−(CF_x), and *C*−(CF_x), can be unambiguously assigned to the cyclotriphosphazene end group and the perfluorinated backbone of A20H, respectively. As is evident in Table 4, the grazing/perpendicular ratio of P(2p) is substantially less than those observed for F(1s), *O*−(CF_x), and *C*−(CF_x). These results therefore indicate that the cyclotriphosphazene end group is preferentially situated at the carbon surface while the PFPE backbone lies at the top of the film at the air interface.

The preferential adsorption of the cyclotriphosphazene end group of A20H on the carbon surface is further supported by comparison of the thin film composition determined at the grazing exit with that of bulk A20H. The bulk composition of A20H-1, calculated from the film composition presented in Table 2, is presented in Table 5. The composition of the thin film was determined from the grazing exit data of Table 4 where contributions to the N(1s), *O*−(non-CF_x), and *C*−(non-CF_x) signals from the CN*x* overcoat are subtracted. The degree to which the carbon overcoat contributes to the N(1s), *O*−(non-CF_x), and *C*−(non-CF_x) signals at the grazing exit was ascertained by the high-resolution measurements of the N(1s) signal. We find that 54 ± 2% of the N(1s) signal is attributable to the lubricant end group (lower binding energy peak) and 46% results from the CN*x* overcoat. From the known composition of CN*x*, the overcoat contributions to the measured

Table 5. Comparison of the A20H-1 Composition Determined at Grazing Incidence with That Expected on the Basis of the Structures Given in Table 1[a]

species	thin film composition (at. %)	bulk composition (at. %)	ratio (thin film/bulk)
N	0.94	2.13	0.44
P	0.98	2.13	0.46
C−(H,N,O)	10.06	21.82	0.46
O−(non-CF*x*)	2.19	4.08	0.54
C−(F)	21.75	18.65	1.17
F	50.50	40.85	1.24
O−CF_2	13.60	10.33	1.32

[a] Corrected film composition calculated on the basis of the N(1s) signal being comprised of 54% from the phosphazene end group and 36% from the overcoat. Thin film/bulk ratio clearly indicates a preference for the cyclotriphosphazene end groups to lie nearer to the carbon surface and the PFPE backbone to lie nearer to the air interface.

O−(non-CF_x), and *C*−(non-CF_x) signals were determined to be 30 and 32%, respectively. Subtraction of the overcoat signals from the grazing incidence data in Table 4 yields the thin film composition reported in Table 5. We note that the near equivalence of the corrected nitrogen concentration and the measured phosphorus concentration reported in Table 5, which is consistent with the 1:1 stoichiometry of these species in the bulk lubricant, validates the correction performed. The ratio of the thin film composition to the bulk composition presented in Table 5 clearly indicates that the cyclotriphosphazene end groups of A20H are preferentially located at the carbon surface. However, on the basis of the N(1s), the *C*−(non-CF_x), and the *O*−(non-CF_x) ratios, we cannot establish whether the preferential adsorption of the end group at the carbon surface is driven by an attractive interaction between the surface and the phosphazene ring[26,27] or the phenoxy ligands.[28]

2. Surface Energy and Stability of A20H films on CN*x* Surfaces. The dispersive surface energy (γ^d) for the bare CN*x* overcoat was determined to be 42 mJ/m^2. Upon application of A20H to the CN*x* surface, a decrease in the magnitude of the dispersive surface energy results. The dependence of γ_s^d on the A20H film thickness is shown for both A20H-1 and A20H-2 in Figure 6. The dispersive component of the surface energy is observed to decrease monotonically with increasing lubricant film thickness in the 0−12 Å film

(26) Zhao, Z.; Bhushan, B.; Kajdas, C. *Tribol. Lett.* **1999**, *6*, 141.
(27) Kasai, P. H. *J. Inf. Storage Proc. Syst.* **1999**, *1*, 23.
(28) Waltman, R. J.; Lengsfield, B.; Pacansky, J. *Chem. Mater.* **1997**, *9*, 2185.

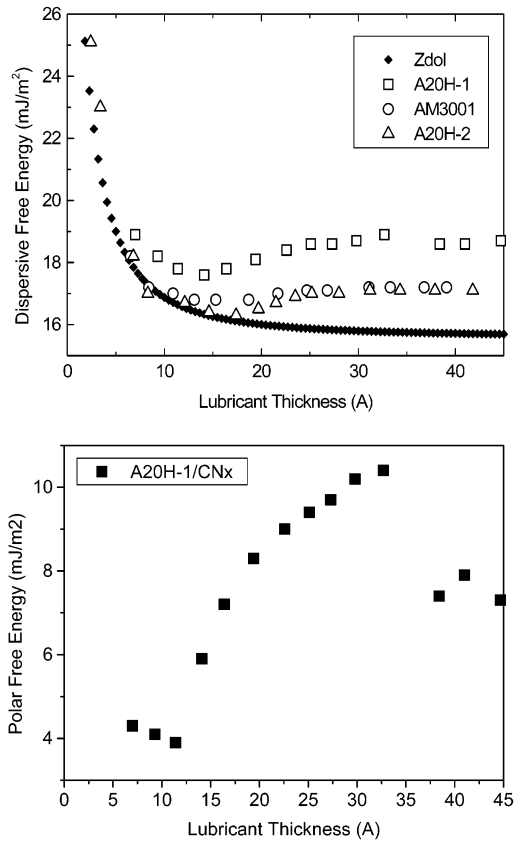

Figure 6. (Top) The dispersive surface energy of A20H-1, A20H-2, Zdol 4000, and AM3001 as a function of lubricant film thickness on CN*x*. (Bottom) The polar surface energy of A20H-1 as a function of lubricant film thickness on CN*x*.

thickness range. The dispersive surface energy then increases as the film thickness is increased over the range $13 \leq h \leq 50$ Å for A20H-1 and $15 \leq h \leq \sim 45$ Å for A20H-2. The surface energy then becomes invariant with further application of A20H. From the asymptotic value of the surface energy at the highest film thicknesses studied, the bulk surface tension of A20H-1 (18.6 mJ m^{-2}) is approximately 10% greater than that of the A20H-2 sample (17.2 mJ m^{-2}). This is consistent with the difference in molecular weights between the two samples. In particular, by virtue of the higher molecular weight of A20H-2 compared to that of A20H-1, the PFPE backbone will comprise a larger fraction of the lubricant structure. Given that the dispersive surface energy of the PFPE backbone (15.6 mJ/m^2) is much less than that of the end group (the dispersive surface energy of neat X-1P on CN*x* is 36 mJ/m^2), the lower surface energy measured for A20H-2 would be expected.

The observed dependence of the A20H-1 dispersive surface energy on film thickness is qualitatively similar to that previously reported for carbon surfaces lubricated with other perfluoropolyether structures.[6,29,30] This is illustrated in Figure 6 where analogous surface energy data is presented for the Zdol/CN*x* and AM3001/CH*x* systems. The minimum observed in the A20H free energy vs film thickness at nominally 13 Å (A20H-1)

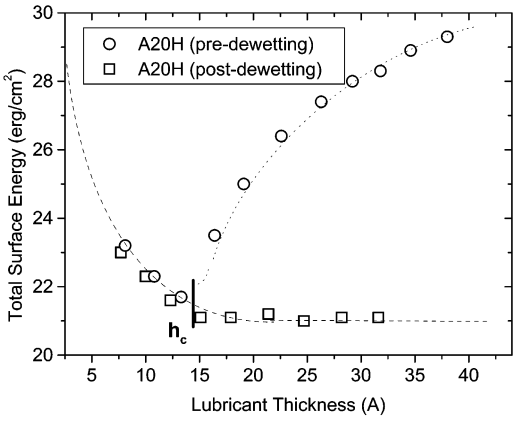

Figure 7. Total surface energy (dispersive + polar) for A20H before and after dewetting above the critical dewetting thickness, h_c.

and ~15 Å (A20H-2) is reflective of an adhesive interaction between the CN*x* surface and the A20H film. The absence of an analogous minimum in the Zdol/CN*x* system indicates that the attractive dispersive interaction involves the cyclotriphosphazene end group of A20H. We note that the presence of this attractive interaction is consistent with the XPS results, indicating a preferential adsorption of the cyclotriphosphazene derivative onto the carbon surface.

The polar component of the surface energy for the CN*x* overcoats used in this work is nominally 14 mJ/m^2. The origin of the polar sites detected at the CN*x* surface has been previously attributed to the presence of carbon−oxygen and carbon−nitrogen functionalities.[6] Application of an A20H film to the CN*x* overcoat strongly impacts the surface polarity. The polar surface energy for A20H-1 is shown in Figure 6 (bottom) as a function of film thickness. The addition of the lubricant to the surface in the thickness range of 0−12 Å results in a decrease in the surface polarity. When the film thickness is increased further, however, the magnitude of the polar component of the surface energy increases substantially. This oscillatory dependence on applied A20H film thickness is completely analogous to that previously reported for the Zdol/CN*x*,CH*x* systems.[6,29−31] The initial decrease in the polar surface energy is reflective of an attractive, polar interaction between the A20H lubricant and the polar sites on the CN*x* surface. Given that the PFPE backbone is apolar (and hence incapable of a polar interaction), the observed surface energy decrease indicates that the hydroxyl end group interacts with the surface. When the A20H lubricant thickness exceeds full monolayer coverage, a number of the lubricant end groups will not be able to access the polar surface sites and the measured polarity increases (Figure 7).

A consequence of the oscillatory dependence of the A20H surface energy on film thickness is that the stability of the lubricant film will be film-thickness-dependent. For example, for A20H-1 films in the monolayer thickness regime ($h \lesssim 13$ Å), the decreasing surface energy with increasing film thickness will drive the complete wetting of the carbon surface by the lubricant film. However, for films in the thickness

(29) Tyndall, G. W.; Leezenberg, P. B.; Waltman, R. J.; Castenada, J. *Tribol. Lett.* **1998**, *4*, 103.
(30) Waltman, R. J.; Zhang, H.; Khurshudov, A.; Pocker, D.; Karplus, M.; York, B.; Thiele, J.-U.; Tyndall, G. W. *Tribol. Lett.* **2002**, *12*, 51.
(31) Waltman, R. J.; Khursudov, A.; Tyndall, G. W. *Tribol. Lett.* **2002**, *12*, 163.

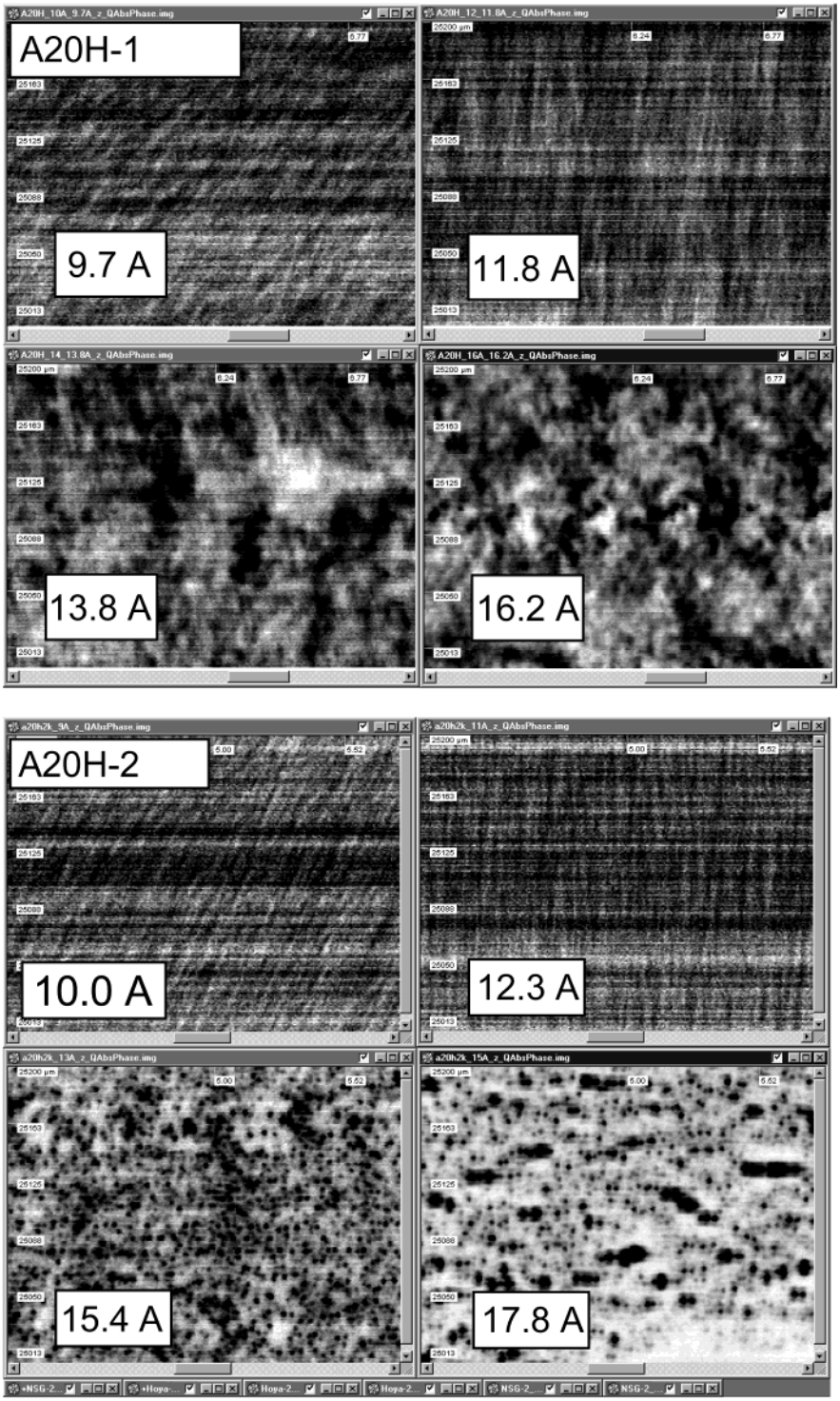

Figure 8. Images of disk surfaces exhibiting lubricant dewetting as a function of film thickness for (top) A20H-1 and (bottom) A20H-2. The dewetting is nominally observed at 11.8 < h < 13.8 Å and 12.3 < h < 15.4 Å for A20H-1 and A20H-2, respectively.

regime of 13 ≤ h ≤ 45 Å, the increasing free energy with increasing film thickness will result in film disjoining pressures that are negative. This indicates that A20H films deposited on carbon surfaces at thicknesses in excess of the first monolayer will be thermodynamically unstable.

The stability of A20H-1 and A20H-2 films on CNx overcoated disks was studied using an optical imaging technique. Representative results are shown in Figure 8. When these films are applied to CNx surfaces at thicknesses less than the critical dewetting thickness (13 Å for A20H-1, ∼15 Å for A20H-2), contiguous (completely wetting) films are always observed. In contrast, when the applied A20H film thickness exceeds the critical dewetting thickness, an autophobic dewetting of the film is observed. This dewetting is apparent in Figure 8 where the light areas in the optical images correspond to an A20H film of monolayer thickness and the dark spots correspond to locally thicker regions of the lubricant. The autophobic dewetting of A20H films in excess of the critical dewetting thickness is not always spontaneous, however. This is shown in Figure 9 for two A20H-2 films deposited on CNx at thicknesses of 17.4 and 24.0 Å. Immediately after lubricant applica-

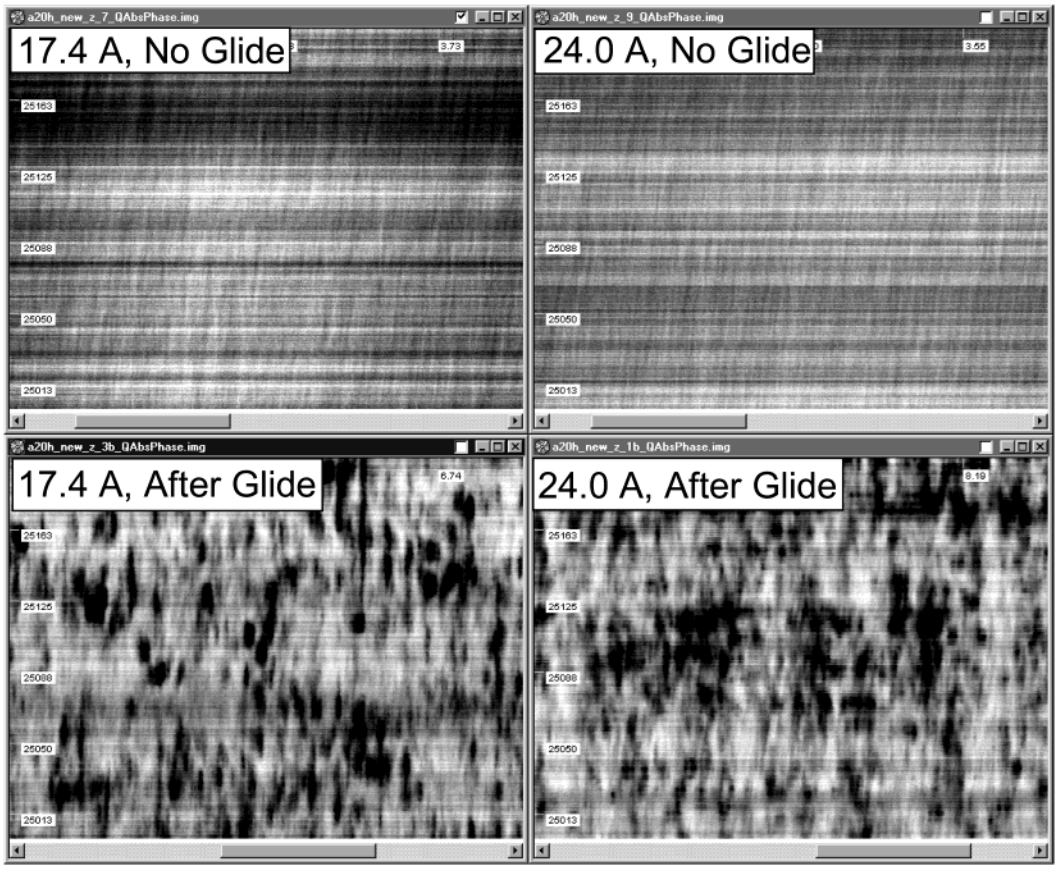

Figure 9. Images showing the dewetting of A20H-2 films > monolayer thickness induced by gliding a head over the disk surface.

tion, both of these films were imaged. As shown in Figure 9 (top), no dewetting is observed. However, when a magnetic recording head is flown over these disks and the surfaces are re-imaged, lubricant dewetting is clearly observed, Figure 9 (bottom). We note that films below the critical dewetting thickness do not dewet under these same conditions.

3. Bonding and Evaporation Kinetics of A20H on CN*x* Surfaces. Exposure of monolayer A20H films to elevated temperature results in the evaporation of a fraction of the initially applied film and an increase in the level of adhesion of the remaining film. This is illustrated in Figure 10, where the results of experiments conducted on A20H-2 (left) and A20H-1 (right) films exposed to temperatures between 64 and 120 °C are presented. The kinetics of bonding and evaporation in monolayer A20H-2 films are analogous to those previously discussed for the bonding and evaporation of monolayer Zdol to CN*x*/CH*x* surfaces.[6,32] In brief, the temporal evolution of the bonding and evaporation profiles are not adequately described using a classical kinetic treatment, but rather require the use of a time-dependent rate "coefficient" of the form

$$k(t) \propto k_0 t^{-h} \qquad (7)$$

where k_0 is the initial rate constant and t is the time. The significance of the functional form of the fractal time dependence h has been discussed previously[32] and is not the focal point of this paper.

The temporal evolution of the A20H evaporation is very similar for both samples studied. The solid lines accompanying the data in Figure 10 are fits obtained using a rate coefficient of the form $k(t) = k_0 t^{-1.0}$, with the initial rate coefficient, k_0, being the only adjustable parameter. These results are completely analogous to those previously reported for a variety of monolayer PFPE films.[33] Comparison of the results presented in Figure 10 with those previously reported for Zdol demonstrates that the addition of the cyclotriphosphazene end group to the PFPE backbone does not substantially reduce the evaporation rate at elevated temperatures and thus the molecular weight of the PFPE backbone will have to be adjusted according to the application.

Upon application of a 12 Å film of A20H-2 to the CN*x* surface, nominally 20% (2.5 Å) of the film "bonds" to the surface prior to the start of the kinetic experiments. The fraction of the A20H-1 monolayer bonded to the CN*x* surface immediately following film application (55−60%) is substantially larger than that observed for A20H-2. The reason for this increase in the initial bonded fraction is not known. Upon exposure of both A20H films to elevated temperature, the bonded fraction increases to nominally 0.7−0.8 over the course of 1 week. As shown by the solid line fits to the data, the bonding kinetics are adequately described using a rate coefficient that scales as $k(t) = k_0 t^{-0.5}$.

The kinetic behavior displayed in Figure 10 for the bonding of A20H films to CN*x* is very similar to that

(32) Waltman, R. J.; Tyndall, G. W.; Pacansky, J.; Berry, R. J. *Tribol. Lett.* **1999**, *7*, 91.

(33) Tyndall, G. W.; Waltman, R. J. *J. Phys. Chem. B* **2000**, *104*, 7085.

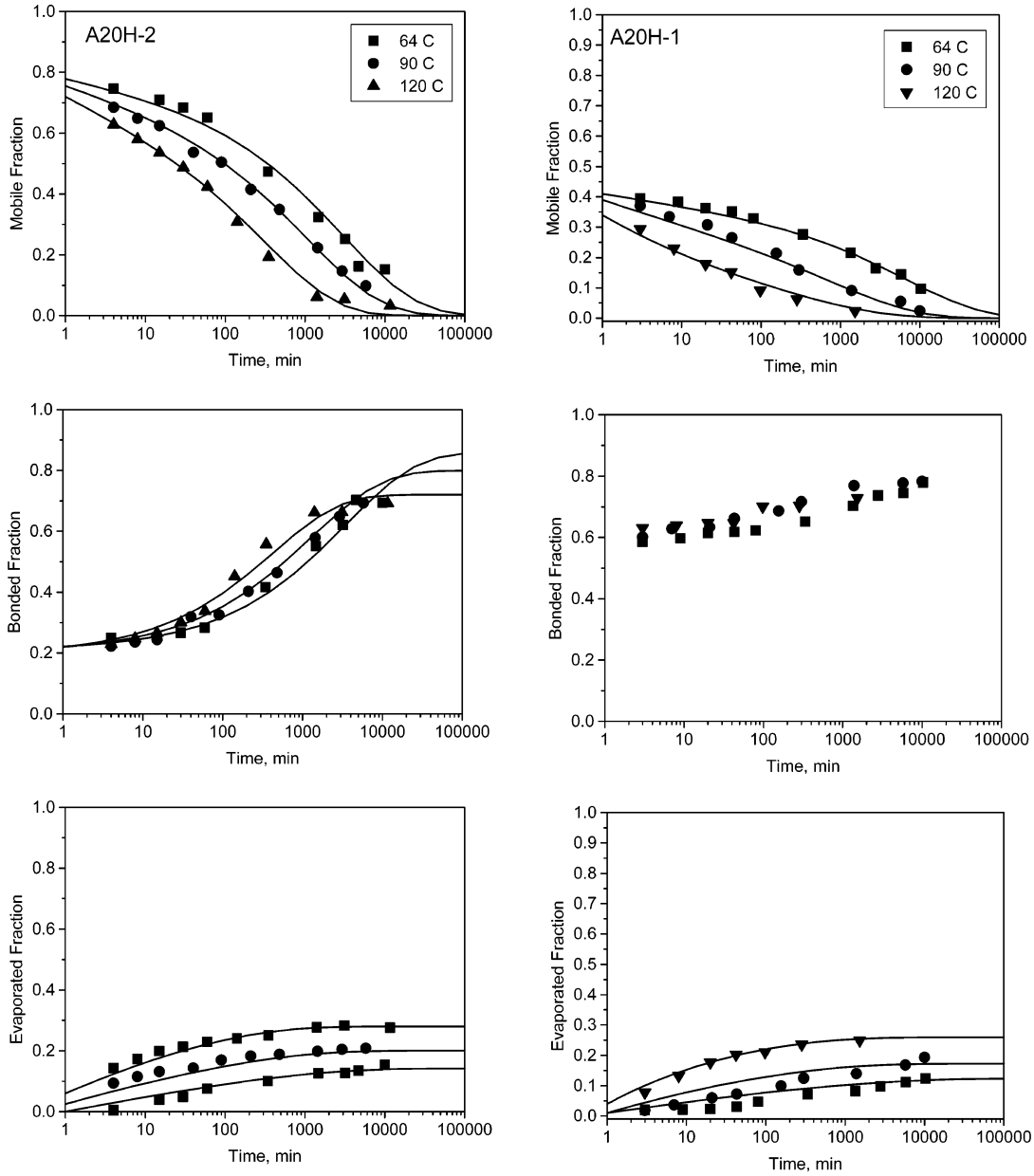

Figure 10. Changes in the (top) mobile, (middle) bonded, and (bottom) evaporated fractions for (left column) 12 Å A20H-2 and (right column) 12 Å A20H-1 on CN*x* as a function of time and temperature between 64 and 120 °C.

previously reported for Zdol. As discussed previously,[6] PFPE structures not containing reactive end groups do not bond to amorphous carbon surfaces. Consequently, the attractive interaction leading to the A20H bonding necessarily involves the end groups. In separate experiments to be discussed in detail elsewhere, the cyclotriphosphazene X-1P does not "bond" to the CN*x* surface when exposed to the same conditions. On the basis of these results, we conclude that the increased adhesion observed in A20H films upon exposure to elevated temperature results from the formation of a hydrogen-bonding interaction between the hydroxyl end group of A20H and the polar sites on the CN*x* surface. We furthermore conclude that the strength of the attractive interaction between the cyclotriphosphazene end group and the carbon surface is of insufficient strength to resist removal via the solvent extraction methodology utilized. We note that this is consistent with the surface energy results. In particular, the depth of the minimum in the dispersive component of the surface energy is reflective of the interaction strength between the cyclotriphosphazene end group and the surface. This minimum is substantially less than that observed in the polar component surface energy, which is reflective of the hydrogen-bonding interaction of the hydroxyl end group.

4. Mobility of Surface-Adsorbed A20H Films. Numerous reports have pointed to the mobility of the disk lubricant mobility as an important criterion for the production of a reliable head−disk interface. In this work, we qualitatively compare the mobility of monolayer A20H films with that of monolayer Zdol films. In particular, experiments are performed which independently probe (a) the rate at which these films reflow into an area of the disk surface that becomes locally depleted of lubricant and (b) the ability of these films to resist film thinning by an applied force.

In the first set of experiments, magnetic recording disks were initially coated uniformly with either A20H or Fomblin Zdol (fractionated $M_n = 2540$). The mobile

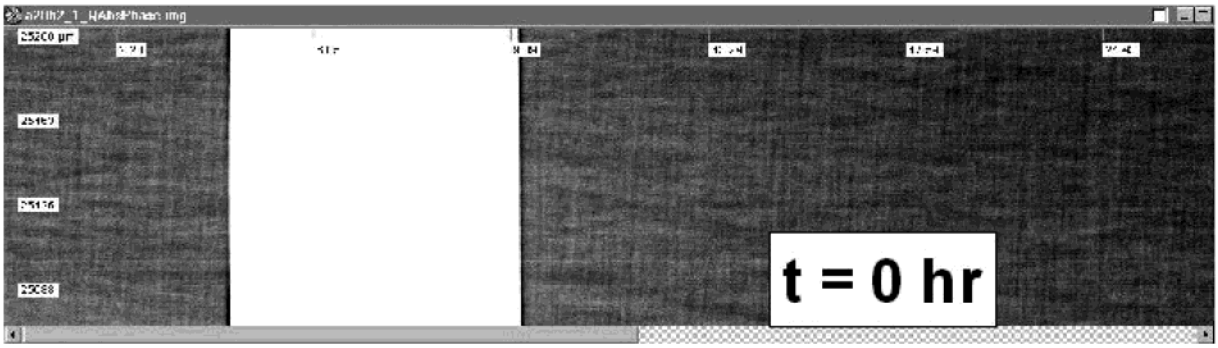

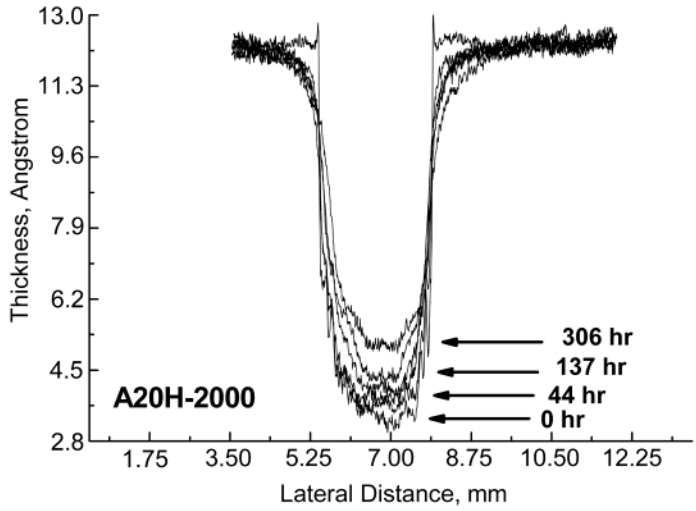

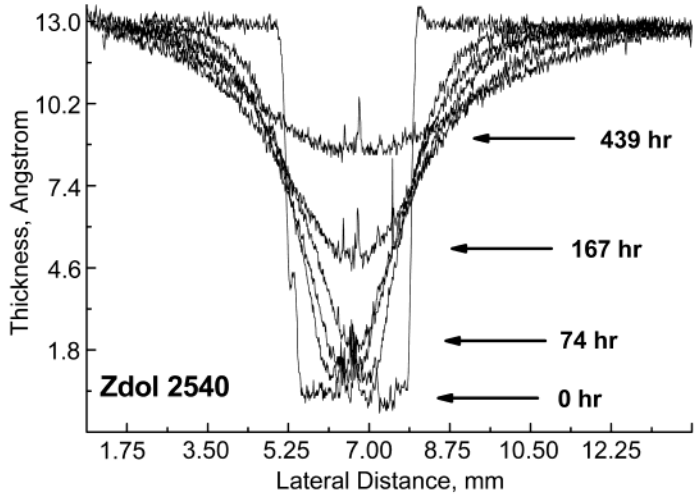

Figure 11. (Top) Image showing the lubricant thickness step (white stripe) for 11.8 Å (2.8 Å bonded) of A20H-2 on CN*x* for the subsequent flow profile studies. (Middle, bottom) Lubricant flow as a function of time on CN*x* at ambient conditions for 11.8 Å (2.8 Å bonded) of A20H-2 and 13.2 Å (1.0 Å bonded) of Zdol 2540. For A20H-2, flow profiles are presented at 0, 16, 44, 69, 137, and 306 h. For Zdol 2540, flow profiles are presented at 0, 24, 47, 74, 167, and 439 h.

fraction of the lubricant film was then removed from a radial "stripe" (approximately 2−4 mm wide) of the disk. The rate at which the lubricant film reflows into the depleted zone of a stationary disk was then followed as a function of time using ellipsometry. In particular, the reflow of an 11.8 Å A20-H film with a bonded film thickness of 2.8 Å was compared with that of a 13.2 Å Zdol 2540 film with a bonded film thickness of 1.0 Å. Figure 11 (top) shows the ellipsometric image of an A20H-2 lubricated disk surface following removal of the mobile film. The white stripe in the figure corresponds to the region of the disk where all mobile lubricant has been removed. The thickness profile corresponding to this region of the disk is shown in Figure 11 (bottom). As a result of the thickness gradient produced in the lubricant film, a disjoining pressure differential develops that drives lubricant flow into the depleted zone. This reflow is shown in Figure 11 (bottom), where the lubricant film thickness profile in the depleted zone is presented at a series of elapsed times. As is immediately apparent in Figure 11 (bottom), the rate of Zdol reflow into the depleted track is much more rapid than that observed for A20H-2.

The flow of liquids on solid surfaces has been an area of active research in recent years. The macroscopic spreading of liquids on solids has been reviewed by de

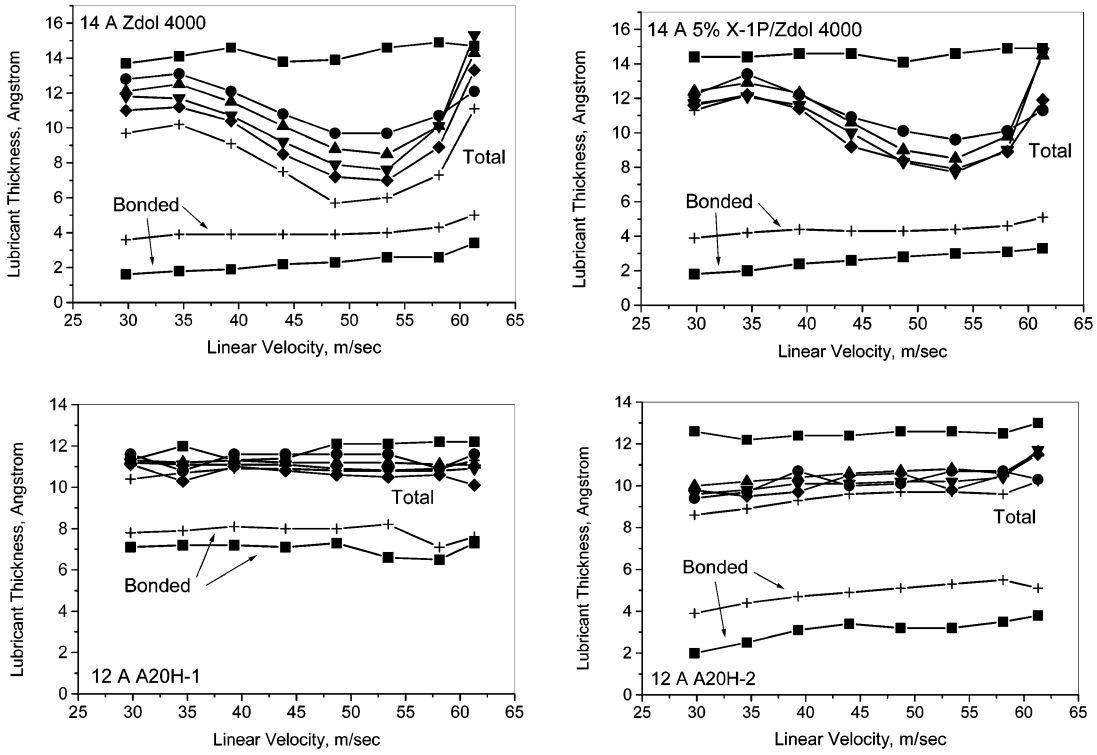

Figure 12. Measured lubricant redistribution on a 84 mm disk (CN*x*) rotating at 15000 rpm as a function of time. (Top, left) 14 Å Zdol 4000; (top, right) 14 Å 5% X-1P/Zdol 4000; (bottom, left) 12 Å A20H-1; (bottom, right) 12 Å A20H-2. The total lubricant thicknesses were measured at 0 (■), 10 (●), 20 (▲), 30 (▼), 40 (◆), and 60 (+) days. The bonded thicknesses were measured at 0 (■) and 60 (+) days. The disks were spun (no head flying) in a disk drive at ambient temperature and humidity (50% RH). The temperature of the base casting of the disk drive was measured to be 40 °C during the 15000 rpm operation.

Gennes.[34] In the film thickness regime of $h \geq 100$ Å, fluid flow is driven by gravitational and capillary forces. In contrast, the flow of molecularly thin liquid films ($h \leq 50$ Å) on surfaces are driven by gradients in the film disjoining pressure, Π. Molecularly thin PFPE film has been shown to scale as[35]

$$R(t) = (D_{\text{eff}}t)^{1/2} \tag{8}$$

where $R(t)$ is the distance traveled by the film in time t and D_{eff} is typically referred to as the effective "diffusion coefficient". We note, however, that since the reflow is driven by a pressure gradient, and hence treated theoretically within the context of a Pouiselle-like flow,[36,37] D_{eff} fundamentally differs from the conventional diffusion coefficient used to describe the random motion of a polymer chain in a bulk liquid. In particular, the effective diffusion coefficient for a confined film can be written as

$$D_{\text{eff}} = -mh\left(\frac{\mathrm{d}\Pi}{\mathrm{d}h}\right) \tag{9}$$

where h is the film thickness and m is the mobility. As is apparent from eq 9, the magnitude of the effective diffusion coefficient is strongly dependent on the film thickness. Since A20H and Zdol films of comparable film thickness and bonded fraction were studied in the current work, our results imply that the mobility of the monolayer A20H film is less than that of the Zdol film.

The lubricant on a rotating magnetic recording disk is subjected to wind shear and centrifugal forces that can induce a migration/redistribution of the film on the disk surface. This phenomenon was studied in the current work by coating magnetic recording disks with initially uniform lubricant films and rotating these disks at room temperature at 15k rpm for times up to 60 days. The radial distribution of the lubricant films on the disks was then quantified using FTIR. We stress that no magnetic recording heads were flown over the rotating disks in these tests.

The impact of disk rotation on monolayer films of three lubricant systems, A20H, Zdol 4000, and a mixture of X-1P(5%) and Zdol 4000, was measured. These films were not annealed prior to use and were initially characterized by a relatively high mobile fraction. The results of these tests are shown in Figure 12. Upon rotation of disks lubricated with either Zdol 4000 or the X-1P/Zdol 4000 mixture, a marked thinning of the lubricant is observed at the radial position of nominally 31 mm (linear velocity ~ 40 m/s). A concomitant buildup of lubricant at the disk outside diameter is also observed. The formation of a distinct minimum in the thickness profiles for both Zdol 4000 and the X-1P/Zdol 4000 mixture clearly indicates that lubricant thinning under the experimental conditions employed is driven by the air shear and/or the centrifugal force generated by the rotating disk. Also shown in Figure 12 is the radial distribution of bonded Zdol on the disk surface. Since this component of the Zdol film is not strongly impacted by the disk rotation, we conclude that lubri-

(34) de Gennes, P. G. *Rev. Mod. Phys.* **1985**, *57*, 827.
(35) Min, B. G.; Choi, J. W.; Brown, H. R.; Yoon, D. Y.; O'Connor, T. M.; Jhon, M. S. *Tribol. Lett.* **1995**, *1*, 225
(36) Cazabat, A. M. *C. R. Acad. Sci. Paris, II* **1990**, *310*, 107.
(37) Cazabat, A. M.; Fraysse, N.; Heslot, F. *Colloid Surf.* **1991**, *52*, 1.

cant migration induced by disk rotation involves the mobile fraction only. This indicates that the level of adhesion provided by the hydrogen-bonding interaction between the hydroxyl end groups and the surface active sites is sufficient to resist thinning under these conditions.

The results of analogous experiments conducted with A20H-1 and A20H-2 films are also shown in Figure 12. In the case of A20H-1, we observe no significant depletion or redistribution of the initially applied lubricant film. A slight increase in the bonded fraction is observed to occur during the 60 days required to perform the testing. When the A20H-2 film is subjected to the same conditions, a small decrease in the total lubricant thickness is observed. However, unlike the redistribution found in the Zdol-based systems, the radial distribution of both A20H films is uniform across the entire disk surface under the test conditions employed. Thus, while the air shear and/or the centrifugal force generated by the rotating disk is of sufficient magnitude to cause redistribution in the Zdol system under the conditions employed, it is insufficient to drive flow in the mobile fraction of the A20H films. We attribute this to the increased adhesion provided by interaction of the cyclotriphosphazene end group with the carbon surface in the A20H films.

Discussion

The results described above indicate that the PFPE polymer chains in monolayer A20H films adopt structures on the CN*x* surface that result in a majority of both the cyclotriphosphazene and hydroxyl end groups preferentially situated at the carbon surface. While this energetically favorable orientation results from the attractive interactions of both end groups with the surface, the nature and strength of these interactions differ substantially.

The interaction of the hydroxyl end group of A20H with the CN*x* surface is the result of a hydrogen-bonding interaction with the polar sites on the CN*x* surface. The strength of this hydrogen-bonding interaction, which is reflected in the depth of the polar surface energy minimum, is of sufficient strength to render the hydrogen-bonded fraction of the film inextractable with good solvents. It furthermore limits both the evaporation and the mobility of the A20H lubricant on the CN*x* surface. The minimum in the dispersive component of the surface energy on A20H film thickness indicates that the attraction between the cyclotriphosphazene end group and the CN*x* involves either dipole−dipole (Keesom) or dipole−induced dipole (Debye) interaction forces. A comparison of the depth of the dispersive, nominally 1.0 ± 0.2 mJ m^{-2}, and polar surface energy minima, 3.2 ± 0.4 mJ m^{-2}, indicates that the strength of this dispersion interaction is substantially less than that of the hydrogen-bonding interaction of the hydroxyl end group. This is consistent with the observation that the cyclotriphosphazene−surface interaction alone does not preclude the evaporation of the mobile fraction, nor is it of sufficient strength to preclude extraction with good solvents. The impact of this interaction is manifested, however, in the substantially reduced mobility of the nonbonded fraction of the A20H lubricant film. This is discussed in more detail below.

Ab initio calculations focusing on the identification of the reactive sites in a series of cyclotriphosphazene structures including X-1P have been reported.[28] The results of these studies indicate that the cyclotriphosphazene ring is very reactive as a result of the polar, almost zwitterionic character of the P−N bond which polarizes the nitrogen atom negatively (see discussion above) and the phosphorus atom positively. While the cyclotriphosphazene ring is, in principle, capable of relatively strong acid−base interactions with the polar active sites on the carbon surface, we find no evidence for this type of reaction with either X-1P[38] or A20H. We attribute this to the presence of the bulky phenoxy ligands, which limits access of the phosphazene ring to the CN*x* surface sites. This then suggests that the observed interaction involves either the lone pairs of electrons on the phenoxy oxygen atom or the aromatic π system. AM3001 is a PFPE lubricant based on the Fomblin Z backbone and terminated with an end group that contains both an oxygen atom with unpaired electrons, and aromatic π system.[39] The dispersive surface energy previously measured for the AM3001/CH*x* system is shown in Figure 6. In both the AM3001 and the A20H systems, minima of comparable depth are observed at nominally the same film thicknesses. On the basis of this similarity, we conclude that the adhesive interaction in monolayer A20H films results from the presence of a dipolar interaction involving the phenoxy ligand and the carbon surface.

The oscillatory dependence of the surface free energy on A20H film thickness indicates that the lubricant forms layers on the carbon surface. This layering will impact the wettability, and hence the stability of molecularly thin A20H films. The wettability of a solid surface by a bulk liquid film on a solid surface is governed by the spreading coefficient, S, which is defined as[34]

$$S = \gamma_s, \gamma_l, \text{ and } \gamma_{sl} \tag{10}$$

where γ_s, γ_l, and γ_{sl} are the surface energy of the solid surface, the surface energy (tension) of the liquid film, and the interfacial interaction free energy, respectively. From eq 10 it follows that a liquid will completely wet a solid surface when $S > 0$, but will only partially wet the surface, that is, form a finite contact angle with the surface, when $S < 0$. Equivalently stated, if the addition of a liquid to the surface results in a decrease (increase) in the free energy of the surface, then the liquid will be completely (partially) wetting. This latter definition is more germane to the present discussion of molecularly thin A20H films. As a result of the oscillatory dependence of the film free energy, the wettability of A20H on a carbon surface will be dependent on the applied film thickness. In the monolayer film thickness regime, for example, $h \leq 13$ Å for A20H-1, the total surface energy decreases with increasing film thickness. The positive disjoining pressure generated in these films will drive the complete wetting of A20H on the carbon surface. For A20H-1 films in the thickness regime of 13 Å $\leq h \leq$ 35 Å, however, the surface energy increases with increasing A20H-1 thickness. This indicates that

(38) These results will be published separately elsewhere.
(39) The structure of AM3001 can be found in ref 3.

the second A20H monolayer is only partially wetting on the first. While A20H films applied to the CN*x* surface at these thicknesses initially appear contiguous, the negative disjoining pressure characteristic of this film thickness regime eventually drives a dewetting of the second monolayer from the completely wetting first. This autophobic dewetting is analogous to that observed in Zdol films cast at thicknesses greater than the first monolayer.[31] Since this dewetting has been previously shown[31] to significantly reduce the effective clearance between a flying head and the rotating disk in magnetic storage devices, the A20H monolayer (13 Å for A20H-1, 15 Å for A20H-2) should be considered as the maximum useable film thickness for this application.

We now focus on the implications of the current studies to the tribology of the head−disk interface. As discussed briefly above, the PFPE lubricant at the head−disk interface in a magnetic storage device is subjected to a number of forces. These include the air-bearing force under the flying slider, the centrifugal force generated by the rotating disk, and the force generated when the head and disk come into physical contact. The ability of the lubricant to resist displacement by these forces, and the ability of the lubricant to reflow into any depleted zone that may be created as a result of these forces, both contribute to the overall durability of the head−disk interface.

The most thermodynamically stable A20H film is one in which the cyclotriphosphazene structural moiety is located preferentially at the carbon surface. While this is similar to that reported for the additive-based X-1P/Zdol system on CN*x*,[40] the mobility of the PFPE lubricant in these two systems are quite different. As discussed above, we find the reflow rate characteristic of the X-1P/Zdol system to be far greater than that of the A20H lubricant, but the ability of the A20H to resist displacement greatly exceeds that of the X-1P/Zdol system. On the basis of these results, we would expect the A20H film to be less durable compared to the more mobile X-1P/Zdol in contact start−stop testing. However, in long-term flyability testing, especially at high rpm, we would expect the A20H to exhibit superior performance. This brief discussion illustrates that the performance of the disk lubricant can be highly dependent upon the precise test methodology used in its evaluation. Furthermore, the optimum disk lubricant for a particular hard-disk drive will be dictated in large measure by the specifics of the drive design, for example, the disk rotational velocity, the diameter of the disk, and the slider fly height.

(40) Mate, C. M.; Kasai, P. H.; Tyndall, G. W.; Lee, C. H.; Raman, V.; Pocker, D. J.; Waltman, R. J. *IEEE Trans. Magn.* **1998**, *34*, 1744.

Conclusions

The goal of these studies was to provide insight into the structure of molecularly thin A20H films adsorbed on CN*x* surfaces. While the low surface tension characteristic of the perfluoropolyether backbone of A20H favors the complete wetting of this lubricant on the carbon surface at all film thicknesses, interaction of the end groups with the carbon surface induces a layering in the adsorbed A20H films. Monolayer A20H films adopt a structure in which both the cyclotriphosphazene and the −OH end groups preferentially orient toward the CN*x* surface. This orientation is thermodynamically driven by the attractive hydrogen-bonding and dipolar interactions that develop between the carbon surface and the hydroxyl and cyclotriphosphazene end groups, respectively. Since the second A20H monolayer is only partially wetting on the first monolayer, films cast in this thickness regime are prone to undergo an autophobic dewetting. The onset of this dewetting can be used to establish a maximum useable A20H thickness for magnetic recording applications.

The preferential adsorption of the cyclotriphosphazene end group of A20H at the carbon interface is similar to that reported previously for the additive-based X-1P/Zdol lubricant system. On the basis of the film mobilities measured in this work, however, the tribology displayed by the X-1P/Zdol and the A20H lubricant systems would be expected to be quite distinct. In the case of the A20H, interaction of the cyclotriphosphazene end group with the CN*x* surface reduces the mobility of the lubricant. As a result of the reduced capacity of this lubricant to reflow into areas of the disk that may become depleted of lubricant following contact with the flying head, the durability of this system could in many tests be less than that of the highly mobile X-1P/Zdol system. The enhanced ability of the A20H films to resist thinning when exposed to an external force could, however, be beneficial in an operating disk drive by mitigating both lubricant depletion from under a flying head and by resisting the centrifugal force generated by the rotating disk surface.

CM021048+